Self-consistent calculation of the nuclear composition in hot and dense stellar matter

Shun Furusawa[1,*] and Igor Mishustin[1,2]
[1]*Frankfurt Institute for Advanced Studies, J.W. Goethe University, 60438 Frankfurt am Main, Germany*
[2]*Russian Research Center Kurchatov Institute, Moscow 123182, Russia*
(Received 18 November 2016; revised manuscript received 17 January 2017; published 8 March 2017)

We investigate the mass fractions and in-medium properties of heavy nuclei in stellar matter at characteristic densities and temperatures for supernova (SN) explosions. The individual nuclei are described within the compressible liquid-drop model taking into account modifications of bulk, surface, and Coulomb energies. The equilibrium properties of nuclei and the full ensemble of heavy nuclei are calculated self-consistently. It is found that heavy nuclei in the ensemble are either compressed or decompressed depending on the isospin asymmetry of the system. The compression or decompression has a little influence on the binding energies, total mass fractions, and average mass numbers of heavy nuclei, although the equilibrium densities of individual nuclei themselves are changed appreciably above one-hundredth of normal nuclear density. We find that nuclear structure in the single-nucleus approximation deviates from the actual one obtained in the multinucleus description, since the density of free nucleons is different between these two descriptions. This study indicates that a multinucleus description is required to realistically account for in-medium effects on the nuclear structure in supernova matter.

DOI: 10.1103/PhysRevC.95.035802

I. INTRODUCTION

Hot and dense matter can be realized in core collapse supernovae and mergers of compact stars. The details of these phenomena are not completely clarified yet because of their complexity [1–6]. One of the central problems is the nuclear equations of state (EOSs) of the hot and dense matter both at sub- and supranuclear densities. The EOS provides information on composition of nuclear matter in addition to thermodynamical quantities such as pressure and entropy. The nuclear composition plays an important role to determine the evolution of the lepton fraction through weak interactions [7,8]. This lepton fraction is one of the most critical ingredients for the dynamics and synthesis of heavy elements in these events [9–12].

There are two types of EOSs for the supernova and merger simulations. The single-nucleus approximation (SNA) is the option in which the ensemble of heavy nuclei is represented by a single nucleus. Two standard EOSs widely used for the simulations of core-collapse supernovae: those of Lattimer and Swefty [13] and of Shen *et al.* [14–16] belong to this category. They calculated the representative heavy nucleus described by the compressible liquid drop model and Thomas Fermi model, respectively. In such calculations, in-medium effects on a single nucleus, such as compression and deformation, are taken into account more easily in comparison with the multinucleus EOS. On the other hand, they are not able to provide a nuclear composition, which is needed to estimate weak interaction rates in supernova and merger simulations. Furthermore, even the average mass number and total mass fraction of heavy nuclei may not be correctly reproduced by the representative nucleus alone [17–19].

The other option is the multinucleus approximation (MNA), in which the full ensemble of nuclei is obtained for each set of thermodynamical condition. In recent years, some EOSs with the MNA have been formulated by different research groups. The statistical model for supernova matter (SMSM) EOS [20–22] is a generalization of the statistical multifragmentation model (SMM) successfully used for the description of nuclear fragments produced in heavy-ion collisions [23]. In this model, temperature dependencies of bulk and surface energies are taken into account using the incompressible liquid-drop model (LDM). Hempel and Schaffner-Bielich have also constructed an EOS (HS EOS) based on the relativistic mean field theory (RMF) [18]. In this model, nuclear binding energies as well as nuclear shell effects are based on experimental and theoretical mass data. In the Furusawa-Yamada-Sumiyoshi-Suzuki (FYSS) EOS [19,24,25], the mass formula extended from the LDM was used to describe nuclear shell effects as well as various in-medium effects. As demonstrated in Buyukcizmeci *et al.* [26] by direct comparison, there are very large differences in nuclear composition predicted by these three models, especially at high densities. A hybrid EOS has been provided by G. Shen *et al.* [27], where a multinucleus EOS based on the virial expansion at low densities is matched to a single-nucleus EOS via Hartree approximation at high densities; i.e., MNA is employed only in the low density regime. An interesting approach has been developed recently [28] wherein the Thomas-Fermi description of individual nuclei was confined with the full nuclear ensemble calculations.

The purpose of the present study is to investigate in-medium effects in a multinucleus description. The in-medium effects on nuclear binding energies are investigated mainly in SNA; Papakonstantinou *et al.* [29] have used the local density approximation and Aymard [30] used the extended Thomas-Fermi approximation. They showed that the binding energies strongly depend on the density and asymmetry of the nucleons in vapor. On the other hand, multinucleus EOSs use very simplified approximations for nuclear binding energies at high densities and temperatures to calculate the statistical ensemble. A fully self-consistent calculation with

*furusawa@fias.uni-frankfurt.de

TABLE I. Bulk properties of nuclear matter [36,37].

Parameter set	n_0 (fm^{-3})	ω_0 (MeV)	K_0 (MeV)	S_0 (MeV)	L (MeV)
B	0.15969	−16.184	230	33.550	73.214
E	0.15979	−16.145	230	31.002	42.498

the multinucleus composition including in-medium effects on nuclear structure has not been done yet due to the complexity. Gulminelli and Oertel [31] have investigated the equilibrium between nucleons and nuclei as well as the nuclear component in multinucleus descriptions, ignoring the in-medium modification of nuclear structure due to the compression and surface interactions with surrounding nucleons.

In the present paper, we take into account self-consistently the compression or decompression of heavy nuclei in the multinucleus description, i.e., the changes of equilibrium densities of individual nuclei embedded in dense stellar environment. Then we evaluate the corresponding changes in the nuclear abundances by the optimization of these equilibrium densities. A comparison of the nuclear equilibration in single- and multinucleus descriptions is also done.

We consider the present work as an attempt to discuss and evaluate several new effects which may appear in dense stellar matter and which have not being analyzed previously. The new EOS we construct in this study is not aimed at immediate practical use in astrophysical simulations, since the required self-consistent calculations need huge computational resources. To reduce the computational cost, the nuclear interactions among nucleon vapor outside nuclei are not considered in the present study, although they are included in many SN EOS via RMF or Skyrme type interactions. In addition, we ignore the shell effect and light clusters other than the α particles. The former is very important to estimate the weak rates at low temperatures $T \lesssim 2$ MeV [8] and the latter also may have influence on the supernova dynamics [32,33]. On the other hand, their theoretical consideration is rather naive and many uncertainties still remain [24,26,34,35]. In fact, at present, nobody can calculate the exact EOS for hot and dense stellar matter starting from first principles. Therefore, we are using a simplified approach which should be considered as a preliminary step for the future work to construct practical and more realistic EOSs for astrophysical simulations.

This article is organized as follows. In Sec. II, we describe our model of EOS, which attempts to solve some of the problems mentioned above. The results are shown in Sec. III. The paper is wrapped up with a conclusion in Sec. IV.

II. MODEL

Total free energy density is represented as

$$f = f_p + f_n + f_\alpha + \sum_i n_i \left(F_i^t + M_i\right), \tag{1}$$

where f_p, f_n, and f_α are the free energy densities of free protons, neutrons, and α particles and n_i, F_i^t, and M_i are the

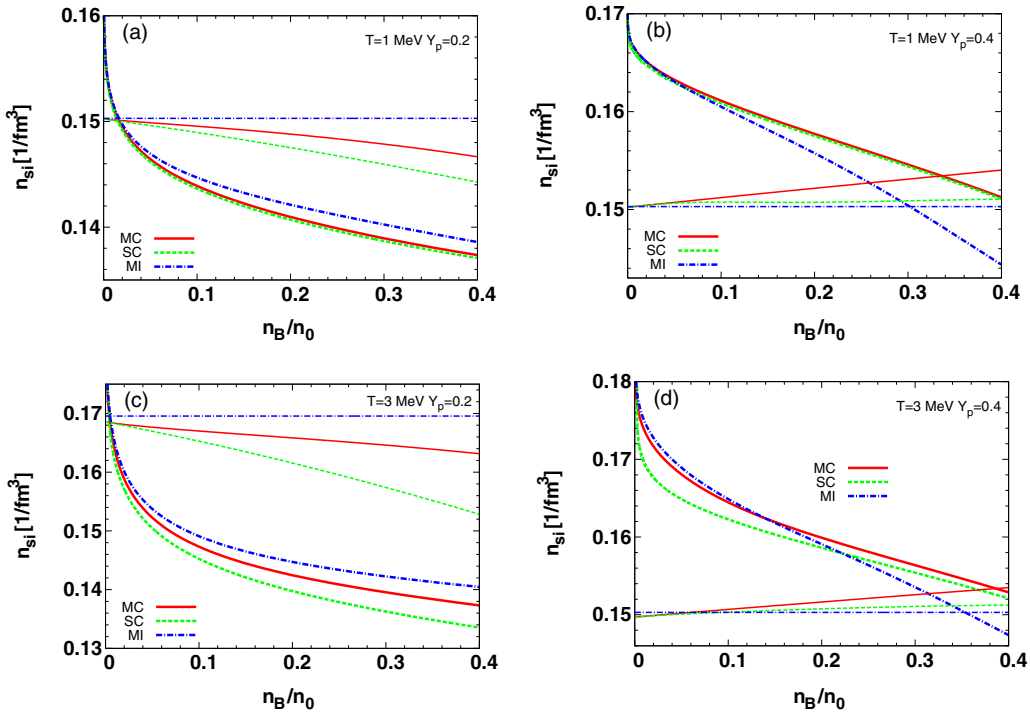

FIG. 1. Average equilibrium density of heavy nuclei for the compressible liquid drop model (Model MC, red solid thick lines) and the incompressible one (Model MI, blue dashed-dotted thick lines) in the multinucleus descriptions, and the equilibrium density of a representative nucleus for the single nucleus EOS with the compressible liquid drop model (Model SC, green dashed lines) as a function of n_B at $T = 1$ MeV (top row) and 3 MeV (bottom row) and $Y_p = 0.2$ (left column) and 0.4 (right column). Thin lines indicate individual equilibrium densities of $^{50}_{20}$Ca at $(T, Y_p) = (3$ MeV$, 0.2)$ and of $^{300}_{100}$Fm at the other conditions for Models MC (red solid lines) and MI (blue dashed-dotted lines). Green dashed thin lines show results for the single-nucleus approximation, in which the representative nucleus is fixed as ^{50}Ca or ^{300}Fm at any density.

number densities, translational free energies and rest masses of individual heavy nuclei i with the proton number $6 \leqslant Z_i \leqslant 1000$. In this study, the light nuclei ($Z \leqslant 5$) are represented by α particles. Other light clusters are ignored, as is usually done in single-nucleus models. This is also needed to make more fair the comparison between MNA and SNA descriptions. The EOS as a function of baryon density n_B, temperature T, and total proton fraction Y_p is obtained by minimizing the free energy density.

Nucleons are considered as structureless pointlike particles moving in the excludedvolume, $V - V_N$, where V is the total volume, V_N is the volume occupied by heavy nuclei, $V_N = \sum_i A_i/n_{si}$, and n_{si} and A_i are the equilibrium density and the mass number of nucleus i. The local number densities of free protons and neutrons are defined as $n'_{p/n} = (N_{p/n})/(V - V_N)$ with the numbers of free protons, N_p, and free neutrons, N_n. The free energy density of free nucleons is obtained as

$$f_{p/n} = (1-V_N/V)n'_{p/n}T\left\{\ln\left(\frac{n'_{p/n}}{g_{p/n}(m_{p/n}T/2\pi\hbar^2)^{3/2}}\right)-1\right\} \quad (2)$$

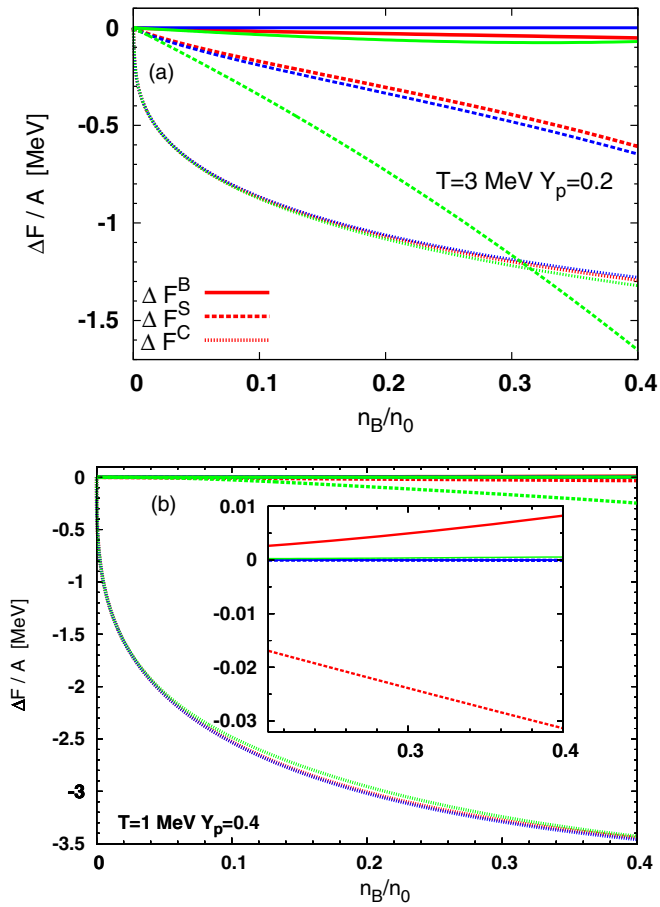

FIG. 2. Energy shifts per baryon in bulk (solid lines), surface (dashed lines), and Coulomb (dotted lines) terms, $\{F_i^{B/S/C}(T,n_e,n'_p,n'_n) - F_i^{B/S/C}(T,0,0,0)\}/A_i$, of ^{50}Ca at $(T,Y_p) =$ (3 MeV,0.2) (top) and of ^{300}Fm at $(T,Y_p) =$ (1 MeV,0.4) (bottom) for Models MC (red lines), MI (blue lines), and SC (green lines).

with $g_{p/n} = 2$ and the nucleon masses $m_{p/n}$. This ideal gas approximation fails at high densities and low temperatures due to nuclear interactions and quantum statistics. However, we believe that the results will not be qualitatively changed, as discussed later. The translational free energy of nuclei i in Eq. (1) is obtained using the expression for the ideal Boltzmann gas with excluded volume correction

$$F_i^t = T\left\{\ln\left(\frac{n_i/\kappa}{g_i(M_iT/2\pi\hbar^2)^{3/2}}\right)-1\right\}, \quad (3)$$

where g_i is the spin degeneracy factors of the ground state, which is set to 1, and $\kappa = 1 - n_B/n_0$.

The calculation below is based on the mass formula used in SMSM and FYSS EOSs, where an additional modification in the symmetry energy has been introduced (parameter L, see below). In this study for simplicity, we neglect the nuclear shell effects, which are derived from nuclear structure calculations of ground states but should be washed out at $T \sim$ 2–3 MeV [25]. The internal free energy of heavy nuclei is assumed to be the sum of bulk, Coulomb, and surface free energies:

$$F_i = F_i^B + F_i^C + F_i^S. \quad (4)$$

We find the equilibrium density of each nucleus, n_{si}, at given T,Y_p,n'_p,n'_n as the baryon density at which the internal free energy of the nucleus takes its minimum value. The nuclear mass in Eq. (1) is defined as

$$M_i = Z_i m_p + (A_i - Z_i)m_n + F_i, \quad (5)$$

where F_i is taken at the equilibrium density.

The bulk free energy of nucleus i is evaluated as

$$F_i^B(n_{si},T) = A_i\omega(n_{si},Z_i/A_i,T), \quad (6)$$

where $\omega(n_B,x,T)$ is the free energy per baryon of bulk nuclear matter as a function of baryon density in nuclei n_B, charge fraction $x = Z/A$, and temperature T, which is

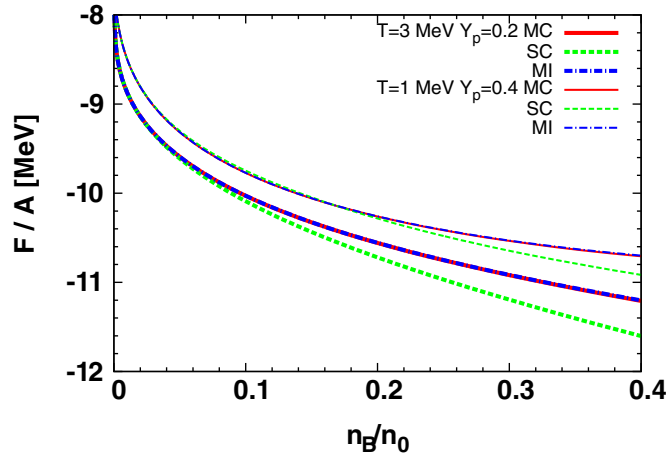

FIG. 3. Internal free energies per baryon, $(F_i^B + F_i^S + F_i^C)/A_i$, of ^{50}Ca at $(T,Y_p) =$ (3 MeV,0.2) (thick lines) and of ^{300}Fm at $(T,Y_p) =$ (1 MeV,0.4) (thin lines), as functions of n_B for Models MC (red solid lines), MI (blue dashed-dotted lines), and SC (green dashed lines).

expressed as

$$\omega(n_B,x,T) = \omega_0 + \frac{K_0}{18n_0^2}(n_B - n_0)^2 + \left[S_0 + \frac{L}{3n_0}(n_B - n_0)\right] \times (1-2x)^2 - \frac{T^2}{\epsilon_0}, \quad (7)$$

with $\epsilon_0 = 16$ MeV [13,23]. We adopt the parameters for bulk properties at zero temperature, ω_0, n_0, K_0, S_0, and L from Refs. [36,37], which are summarized in Table I. The parameter set E is the most standard parameter set that reproduces the nuclear masses and radii of stable nuclei in Thomas-Fermi calculations [36]. They are used in most calculations in this study, while the comparisons between the parameter sets B and E are also presented. The thermal term, T^2/ϵ_0, comes from the integration over excited states of nuclei, which can be taken in the low-temperature approximation at $T \ll \epsilon_F$, where ϵ_F is the Fermi energy ∼40 MeV at saturation density. Here the slope parameter L accounts for the density dependence of the symmetry energy of nuclei when their equilibrium density deviates from n_0. Its actual value is still rather uncertain. Various predictions have been provided by terrestrial nuclear experiments, theoretical analyses, and astrophysical observations [38–43]. Unfortunately, these constraints do not overlap and the actual value is likely to be larger than 35 MeV and less than 131 MeV. The equilibrium densities of asymmetric nuclei are sensitive to L: larger L leads to smaller saturation density of asymmetric bulk matter,

$$n_{s,\mathrm{bulk}}(x) = n_0 - 3n_0L(1-2x)^2/K_0, \quad (8)$$

at which ω takes its minimum value. The other parameters have also some uncertainties as $n_0 = 0.15$–0.16 fm^{-3}, $K_0 = 240 \pm 20$ MeV, and $S_0 = 29.0$–33.7 MeV [35,42,44,45].

The Wigner-Seitz (WS) cell for each species of nuclei i is set to satisfy the charge neutrality within the volume V_i. The cell also contains free nucleons as a vapor outside the nucleus as well as electrons distributed uniformly in the entire cell. The charge neutrality in the cell gives the cell volume

$$V_i = (Z_i - n_p' V_{Ni})/(n_e - n_p'), \quad (9)$$

where V_{Ni} is the volume of the nucleus in the cell and can be calculated as $V_{Ni} = A_i/n_{si}$ and $n_e = Y_p n_B$ is the number density of electrons. The expression for the Coulomb free energy is obtained within the WS approximation by integrating the Coulomb potential over the cell i containing nucleus (A_i, Z_i):

$$F_i^C(n_{si},n_p',n_e) = \frac{3}{5}\left(\frac{3}{4\pi}\right)^{-1/3} e^2 n_{si}^2 \left(\frac{Z_i - n_p' V_{Ni}}{A_i}\right)^2 \times {V_{Ni}}^{5/3} D(u_i), \quad (10)$$

where $u_i = V_{Ni}/V_i$, $D(u_i) = 1 - \frac{3}{2}u_i^{1/3} + \frac{1}{2}u_i$, and e is the elementary charge. Note that the formation of nuclear pasta phases is not taken into consideration in this study. They are essential as intermediate states in the transition to uniform

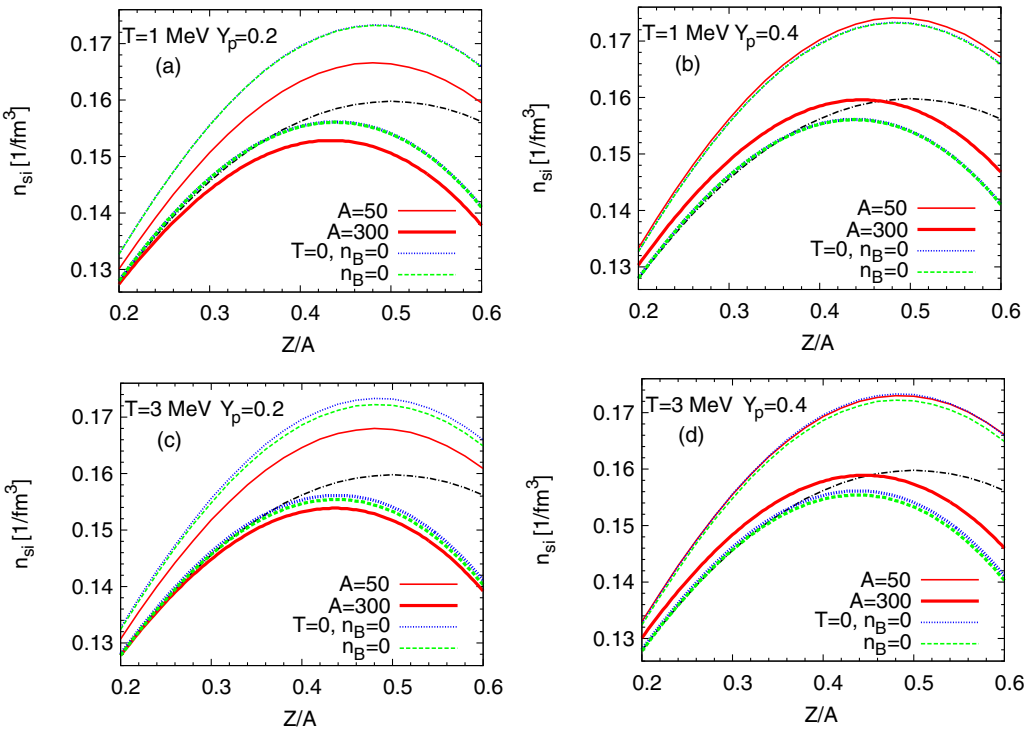

FIG. 4. Equilibrium densities of the nuclei with $A = 50$ (thin) and 300 (thick) as a function of proton fraction in nuclei, Z/A, at $n_B = 0.3\,n_0$ for $T = 1$ MeV (top row) and 3 MeV (bottom row) and $Y_p = 0.2$ (left column) and 0.4 (right column). Red solid lines are those obtained in Model MC, $n_{si}(T,n_e,n_p',n_n')$. Blue dotted and green dashed lines indicate those in vacuum (or in Model MI), $n_{si}(0,0,0,0)$, and those at finite temperature and zero density, $n_{si}(T,0,0,0)$, respectively. Black dashed-dotted lines are the density corresponding to the minimum of bulk free energy ω as a function of charge fraction $x = Z/A$, $n_{s,\mathrm{bulk}}(Z/A)$.

nuclear matter [46–50]. Although their realistic calculation in MNA is rather complicated, they are taken into account phenomenologically in the FYSS EOS. Also, the electron distribution deviates from the uniform one, especially in the nuclear pasta phases [51,52]. However, in this paper, we address the densities at $n_B \lesssim 0.3 n_0$, where these effects are not very important.

The surface free energy is evaluated by the expression generating the one form [23]

$$F_i^S(n_{si}, n'_p, n'_n, T) = 4\pi r_{Ni}^2 \sigma_i \left(1 - \frac{n'_p + n'_n}{n_{si}}\right)^2 \left(\frac{T_c^2 - T^2}{T_c^2 + T^2}\right)^{5/4}, \quad (11)$$

where $r_{Ni} = (3/4\pi V_i^N)^{1/3}$ is the radius of nucleus, $T_c = 18$ MeV is the critical point at which the distinction between the liquid and gaseous phase disappears, and

$$\sigma_i = \sigma_0 \frac{16 + C_s}{(1 - Z_i/A_i)^{-3} + (Z_i/A_i)^{-3} + C_s}, \quad (12)$$

where σ_0 denotes the surface tension for symmetric nuclei. The values of the constants, $\sigma_0 = 1.14$ MeV/fm^3 and $C_s = 12.1$ MeV, are taken from Agrawal *et al.* [53]. The last two factors in Eq. (11) describe the reduction of the surface free energy when the density contrast between the nucleus and the nucleon vapor decreases [19], and when the temperature grows.

The free energy density of α particles is represented as $f_\alpha = n_\alpha(F_\alpha^t + M_\alpha)$, where the translational energy is calculated by the same formula as for heavy nuclei, Eq. (3), but the mass is set to be the experimental value without any modifications at high temperature and densities.

The abundances of nuclei as a function of n_B, T, and Y_p are obtained by minimizing the model free energy with respect to the number densities of nuclei and nucleons under the constraints

$$n_p + n_n + 4n_\alpha + \sum_i A_i n_i = n_B, \quad (13)$$

$$n_p + 2n_\alpha + \sum_i Z_i n_i = n_e = Y_p n_B. \quad (14)$$

In our EOS, the free energy density of nuclei depends on the local number densities of protons and neutrons $n'_{p/n}$. The

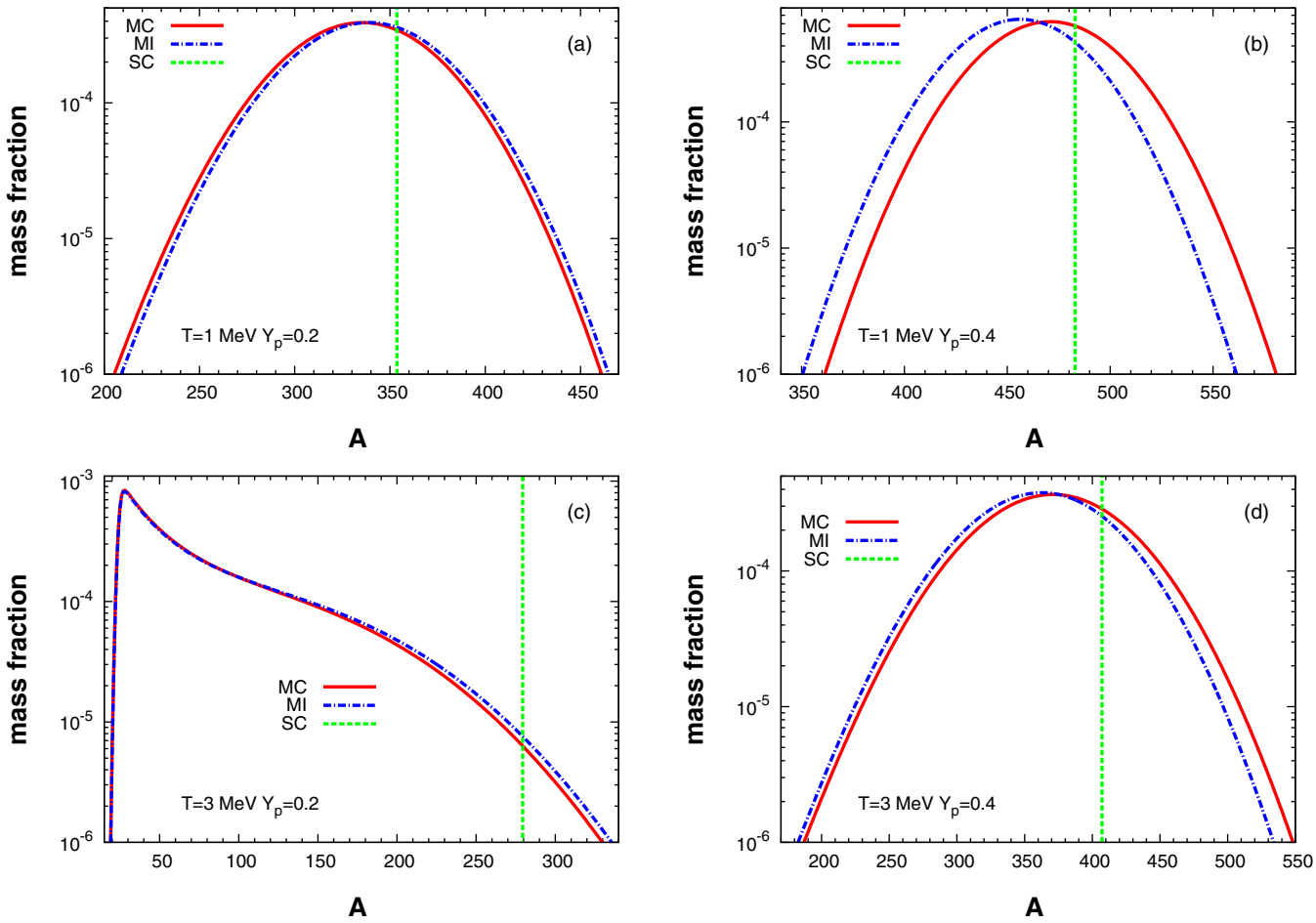

FIG. 5. Mass fractions of elements as a function of mass number for Models MC (red solid lines) and MI (blue dashed-dotted lines) in the multinucleus description at $T = 1$ MeV (top row) and 3 MeV (bottom row) and $Y_p = 0.2$ (left column) and 0.4 (right column). Vertical green dashed lines display the mass numbers of representative nuclei in the single-nucleus description.

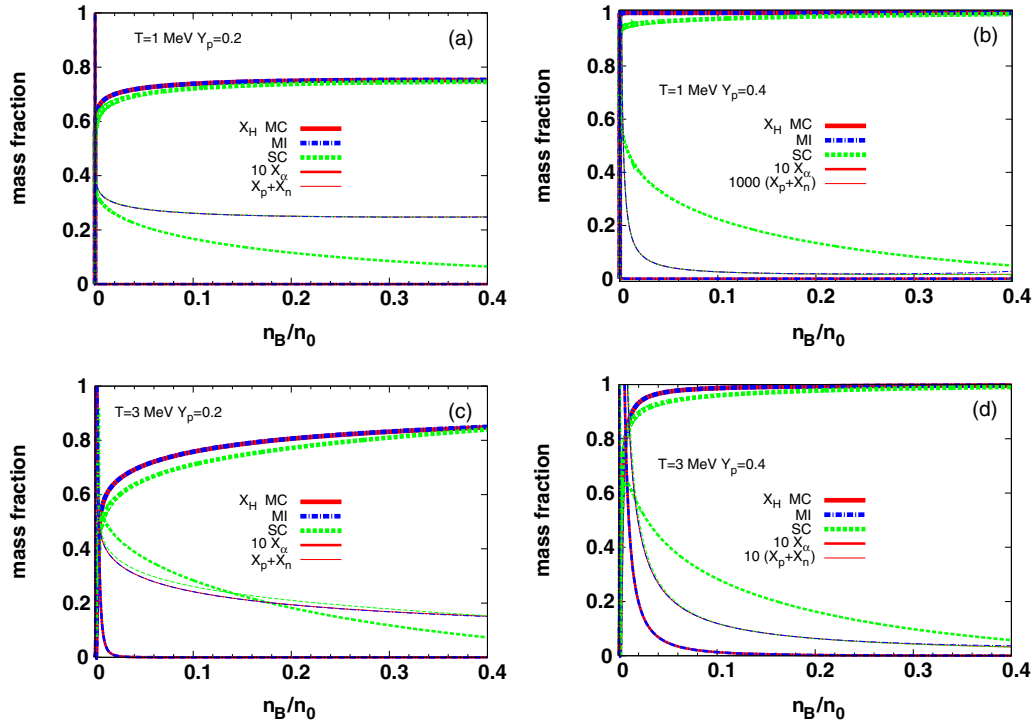

FIG. 6. Mass fractions of heavy nuclei (thick lines), α particles (middle lines), and free nucleons (thin lines) for Models MC (red solid lines), SC (green dashed lines), and MI (blue dashed-dotted lines), respectively, as a function of n_B at $T = 1$ MeV (top row) and 3 MeV (bottom row) and $Y_p = 0.2$ (left column) and 0.4 (right column). Those of alpha particles and/or free nucleons are scaled for best display.

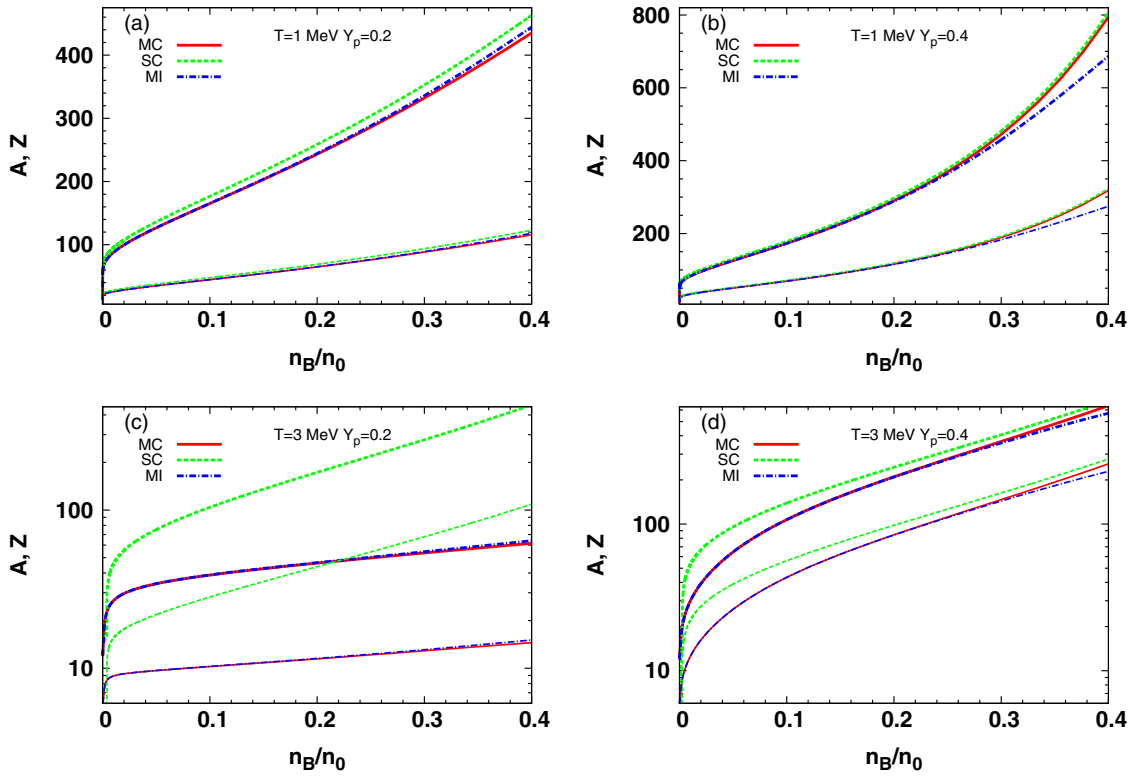

FIG. 7. Average mass and proton numbers (thick and thin lines) of heavy nuclei with $Z \geqslant 6$ for Models MC (red solid lines) and MI (blue dashed-dotted lines) and those of a representative nucleus for Model SC (green dashed lines) as a function of n_B at $T = 1$ MeV (top row) and 3 MeV (bottom row) and $Y_p = 0.2$ (left column) and 0.4 (right column).

nucleon chemical potentials $\mu_{p/n}$ are expressed as follows:

$$\mu_{p/n} = \frac{\partial f}{\partial n_{p/n}} = \mu'_{p/n}(n'_p,n'_n) + \sum_i n_i \frac{\partial F_i(n'_p,n'_n)}{\partial n_{p/n}}, \quad (15)$$

where $n_{p/n} = N_{p/n}/V$, $\mu'_{p/n} = \partial f_{p/n}/\partial n'_{p/n}$ are the chemical potentials of nucleons in the vapor, and the second term originates from the dependence of the free energies of nuclei on $n'_{p/n}$. We hence solve the equations relating $\mu_{p/n}$ and $n'_{p/n}$, Eq. (15), as well as the two constraint equations, Eqs. (13) and (14), to determine the four variables μ_p, μ_n, n'_p, and n'_n.

For comparison, in addition to the compressible liquid drop model in the multinucleus description (Model MC), which has been explained above in this section, we have considered two other simplified EOSs. The first EOS corresponds to the incompressible liquid drop model in the multinucleus description (Model MI), where the equilibrium density of each nucleus is assumed to be fixed to the corresponding value in vacuum, i.e,. $n_{si}(T,n_e,n'_p,n'_n) = n_{si}(0,0,0,0)$. The other is the single-nucleus EOS with the compressible liquid drop model (Model SC), in which the mass and proton numbers of a representative nucleus, $A_{\rm rep}$ and $Z_{\rm rep}$, are introduced instead of an ensemble of nuclei. In this case, the free energy density is expressed as $f = f_p + f_n + f_\alpha + n_{\rm rep}(F^t_{\rm rep} + M_{\rm rep})$ instead of Eq. (1), where $n_{\rm rep}$, $F^t_{\rm rep}$, and $M_{\rm rep}$ are the number density, translational free energy, and mass of a representative nucleus. To find six unknowns, μ_p, μ_n, n'_p, n'_n, $A_{\rm rep}$, and $Z_{\rm rep}$, we use the constraints of Eqs. (13)–(15) and two definitions $\partial f/\partial A_{\rm rep}|_{Z_{\rm rep}} = n_{\rm rep}\mu_n$ and $\partial f/\partial Z_{\rm rep}|_{A_{\rm rep}} = n_{\rm rep}(\mu_p - \mu_n)$. The former and latter may be regarded as surrogates for the multinucleus EOSs (SMSM, HS, FYSS EOSs) and single nucleus EOSs (STOS, LS EOSs) for supernova matter, although various parts in free energies of nucleons and nuclei used by different authors are quite different from each other.

III. RESULTS

Below we present reults for the typical stellar conditions $(T,Y_p) = (1\ \text{MeV},0.2)$, $(1\ \text{MeV},0.4)$, $(3\ \text{MeV},0.2)$, and $(3\ \text{MeV},0.4)$. Figure 1 displays the equilibrium density of a representative nucleus in the single-nucleus EOS and the average values for multinucleus ensembles. On the whole, the ensemble-averaged equilibrium densities decrease as the baryon density increases, since nuclei with larger mass numbers are allowed, and they have smaller equilibrium densities. The equilibrium densities of the nuclei with $(A_i,Z_i) = (50,20)$, $^{50}_{20}$Ca, for $(T,Y_p) = (3\ \text{MeV},0.2)$ and with $(A_i,Z_i) = (300,100)$, $^{300}_{100}$Fm, for the other conditions are also shown in Fig. 1. In the SNA, the representative nucleus at any density is assumed to be the nucleus with $(A_{\rm rep},Z_{\rm rep}) = (50,20)$ or $(300,100)$ described by the compressible liquid drop model. In the MNA, n_{si} of ^{50}Ca or ^{300}Fm is obtained by calculating the whole ensemble of nuclei. We find that the individual nucleus in Model MC is compressed for $Y_p = 0.4$ due to the reduction of Coulomb free energy by the surrounding electrons as the baryon density increases. On the other hand, in a neutron-rich system with $Y_p = 0.2$, the equilibrium densities of nuclei decrease due to two reasons: (a) the impact of electrons on Coulomb free energies is less strong than for $Y_p = 0.4$ and (b) surface energies of nuclei are reduced because of the dripped neutrons. At nonzero temperatures, surface free energies of nuclei are reduced by the factor $[(T_c^2 - T^2)/(T_c^2 + T^2)]^{5/4}$ in Eq. (12) even at zero density, leading to the equilibrium densities smaller than those in vacuum. Hence, the equilibrium densities in Model MC are smaller than those in Model MI at $T = 3$ MeV and $n_B = 0$. It is found that the equilibrium densities in Model SC both for representative nucleus and for ^{50}Ca or ^{300}Fm are smaller than those in multinucleus EOSs in most cases, since more free nucleons are produced outside the nuclei, reducing the surface energies.

The binding energies of nuclei as well as their equilibrium densities are essentially affected by electrons and free nucleons, especially at high baryon densities. Figure 2 displays the shifts of bulk, surface, and Coulomb free energies of ^{50}Ca for $(T,Y_p) = (3\ \text{MeV},0.2)$ and of ^{300}Fm for

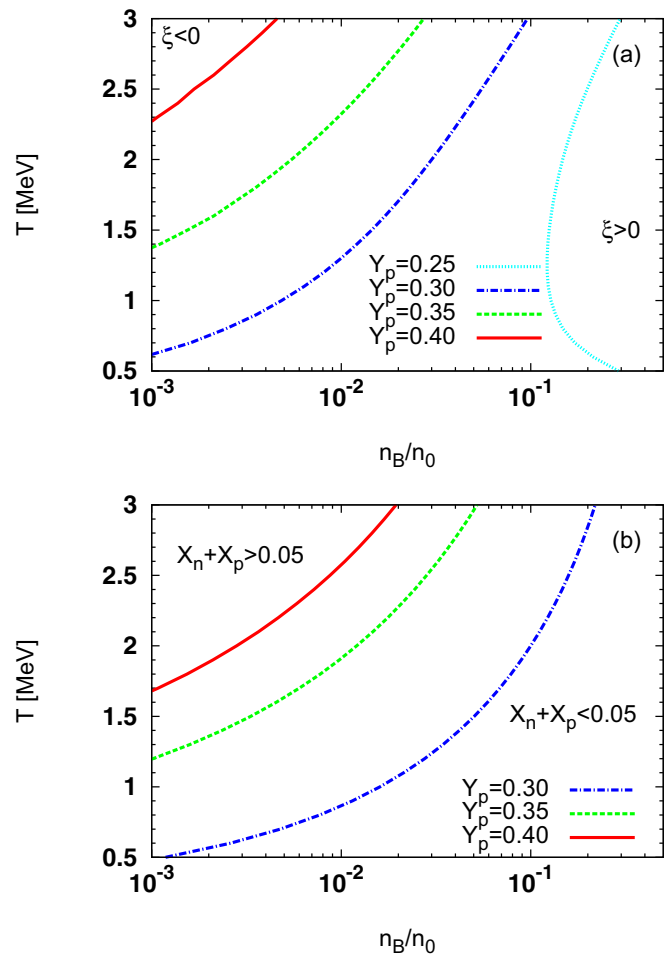

FIG. 8. Critical lines for the compression (top) and mass fraction of free nucleons (bottom) in Model MC for $Y_p = 0.25$ (cyan dotted line), 0.30 (blue dashed-dotted line), 0.35 (green dashed line), and 0.40 (red solid line). They are defined as the compression parameter $\xi = \sum_i n_i(dn_{si}/dn_B)/(\sum_i n_i) = 0$ and the mass fraction of free nucleons $X_p + X_n = 0.05$. The positive value of ξ means that in general the nuclei are compressed. Note that the line of mass fraction for $Y_p = 0.25$ is not displayed, since $X_p + X_n > 0.05$ at all conditions.

$(T,Y_p) = (1\ \text{MeV},0.4)$, $\Delta F_i^{B/S/C} = F_i^{B/S/C}(T,n_e,n_p',n_n') - F_i^{B/S/C}(T,0,0,0)$. The bulk free energies are sensitive to the equilibrium density. Those in Model MI are constant, whereas those in Model MC decrease for $(T,Y_p) = (3\ \text{MeV},0.2)$ and increase for $(T,Y_p) = (1\ \text{MeV},0.4)$ due to the decompression and compression, respectively. The bulk free energy of a representative nucleus in Model SC is always smaller than that in Model MC, since its equilibrium density is smaller. Note that the representative nucleus is assumed to be ^{50}Ca or ^{300}Fm at any density here. In all models, the surface and Coulomb free energies are reduced by free nucleons and electrons, respectively. The equilibrium densities also affect them, as can be seen from the comparison of Models MC and MI; namely, the surface free energies are increased and Coulomb free energies are decreased by decompression for $(T,Y_p) = (3\ \text{MeV},0.2)$ and vice versa for $(T,Y_p) = (1\ \text{MeV},0.4)$.

Figure 3 shows the sum of the bulk, surface, and Coulomb free energies per baryon, the absolute value of which corresponds to the binding energy per baryon, for ^{50}Ca and ^{300}Fm nuclei. Model MC has lower energy than Model MI, due to the compression or decompression. Although the equilibrium densities of nuclei are changed appreciably, as shown in Fig. 1, the changes in binding energies between compressible and incompressible models are rather small. This is because the change of equilibrium density brings not only the reduction of some of the bulk, surface, and Coulomb free energies but also the increase of the others as shown in Fig. 2. On the other hand, the binding energy in Model SC is much larger than in other MNA models, since more free nucleons reduces the surface free energy.

Figure 4 displays the equilibrium densities of some nuclei included in the ensemble of heavy nuclei for Model MC at $n_B = 0.3n_0$, those in vacuum, $n_{si}(T,n_e,n_p',n_n') = n_{si}(0,0,0,0)$, and those at finite temperature and zero density, $n_{si}(T,0,0,0)$. The latter two have almost the same values at $T = 1$ MeV, whereas the finite-temperature modification of surface energies reduces the equilibrium densities notably at $T = 3$ MeV. The nuclei with larger mass numbers have smaller equilibrium densities due to the larger Coulomb repulsion. Also, the neutron-rich nuclei have smaller equilibrium densities, because the additional symmetry energy shifts the minimum point of bulk energy, $n_{s,\text{bulk}}(x)$, to smaller densities. This effect is mainly controlled by the parameter L, which is responsible for the density dependence of the symmetry energy; see Eq. (8). We also find that the nuclei with larger mass numbers are likely to be compressed for $Y_p = 0.4$, since they have large Coulomb energies. As for neutron-rich matter with $Y_p = 0.2$, the nuclei with smaller mass numbers and/or $Z_i/A_i \sim 0.5$ are more strongly decompressed because of the larger surface energies.

The mass fractions of elements as a function of the mass number at $n_B = 0.3n_0$ are displayed in Fig. 5. For $Y_p = 0.4$, Model MC shows a larger mass fraction of nuclei with large mass numbers than Model MI, since they give

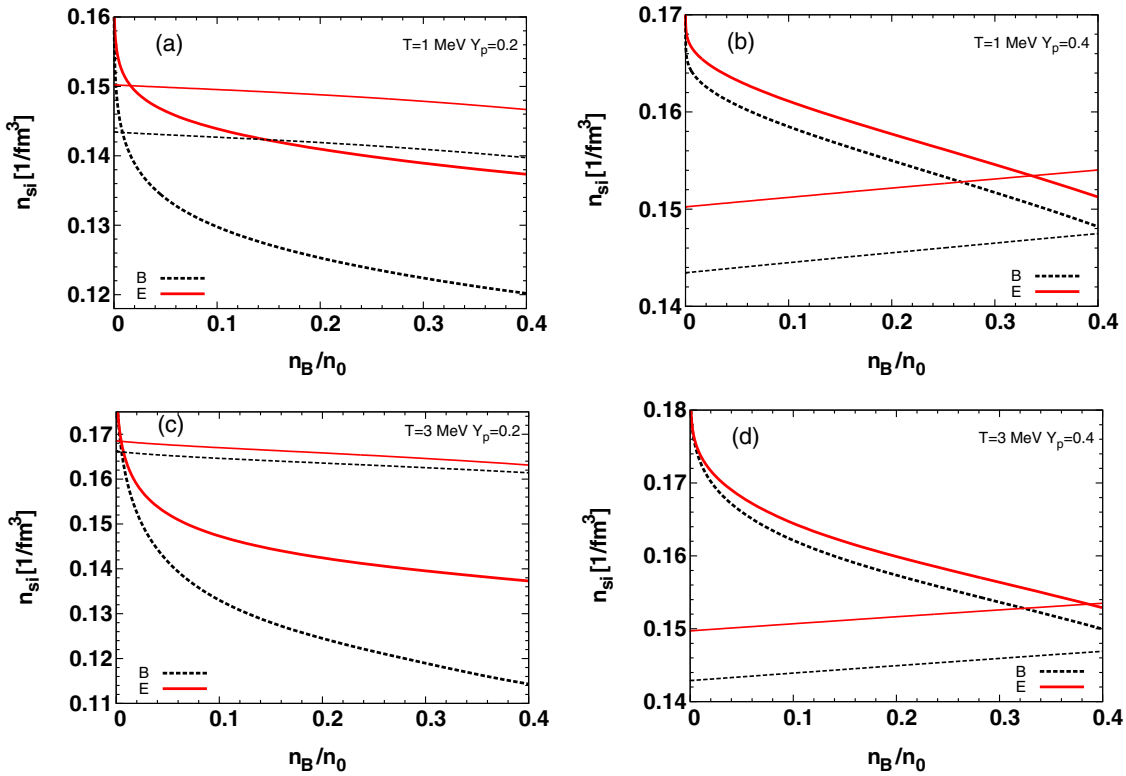

FIG. 9. Average equilibrium density (thick lines) of heavy nuclei as a function of n_B at $T = 1$ MeV (top row) and 3 MeV (bottom row) and $Y_p = 0.2$ (left column) and 0.4 (right column) for MC models with bulk parameter sets B (black dashed lines) and E (red thick lines), the latter of which is identical to the MC model shown in Fig. 1. Thin lines indicate those of $^{50}_{20}$Ca at $(T,Y_p) = (3\ \text{MeV},0.2)$ and $^{300}_{100}$Fm at the other conditions.

larger compressions, as shown in Fig. 4. On the other hand, for $Y_p = 0.2$, the nuclei with smaller mass numbers are more decompressed and more abundant in Model MC. As a result, Model MC predicts nuclei with smaller mass numbers compared to Model MI.

The mass fraction of free nucleons, α particles, and heavy nuclei ($Z_i \geqslant 6$) and average mass and proton numbers of heavy nuclei are displayed in Figs. 6 and 7, respectively, as functions of baryon density. The total mass fraction of heavy nuclei in Model MC is always larger than in Models MI and SC, because of additional degrees of freedom in the description of heavy nuclei. We also find that the mass fractions of α particles are significantly overestimated in Model SC. For $Y_p = 0.4$, Model MC shows the larger mass numbers of heavy nuclei than Model MI, because the formation of such nuclei is favored by the compression, as shown in Fig. 5. On the other hand, for $Y_p = 0.2$, the nuclei with smaller mass numbers are more abundant in Model MC, which leads to the smaller average mass number than that in Model MI. Model SC gives larger mass numbers than multinucleus models, as in Ref. [17]. The deviations of Model SC from Model MC increase with temperature, because nuclei other than the representative nucleus become more and more abundant but the mass fraction of the peak nuclei is reduced.

Figure 8(a) shows the lines in the n_B-T plane separating regions where the nuclei are compressed or decompressed that are determined by the compression parameter $\xi = \sum_i n_i (dn_{si}/dn_B)/(\sum_i n_i)$. The positive value of ξ means that, on average, the nuclei are compressed, and the negative one corresponds to the decompression. The critical lines of the mass fraction of free nucleons $X_n + X_p = 0.05$ are also shown in Fig. 8(b). Note that neutrons are always dripped and $X_n \gtrsim 0.05$ at $Y_p \lesssim 0.25$. Free nucleons are almost diminished and nuclei are dominant at high densities, low temperatures, and high proton fractions. In those states, the nuclei are compressed due to the reduced Coulomb energies. We find that the compression is replaced by decompression when the mass fraction of free nucleons $X_n + X_p$ becomes less than ~0.05–0.15. In core-collpase supernovae and neutron star mergers, such thermodynamical conditions, $n_B \gtrsim 0.01\, n_0$ and $Y_p \gtrsim 0.25$, are usually not realized because of deleptonization [12,54,55]. Therefore, the nuclei are likely to be decompressed due to the presence of dripped neutrons under these conditions. However, during core collapse of massive stars, the nuclei may be compressed due to the surrounding electrons just before the bounce at $n_B \gtrsim 0.3 n_0$, $T \sim 3$ MeV, and $Y_p \sim 0.25$. The parameter ξ is zero in Model MI and negative in Model SC at all densities.

Finally, we discuss the impact of bulk properties on these results by using another bulk parameter set, B, presented in Table I. The major difference between the parameter sets B and E in the bulk properties is the slope parameter L, whereas the same K is assumed. The other parameters S_0, ω_0, n_0 are slightly modified to reproduce properties of stable nuclei [36]. Figures 9 and 10 display the average and individual equilibrium densities for Models MC based on these parameter sets, in which the results for the parameter set E are identical to those in Figs. 1 and 4. Both average and individual equilibrium densities in the model of the parameter set B with larger L

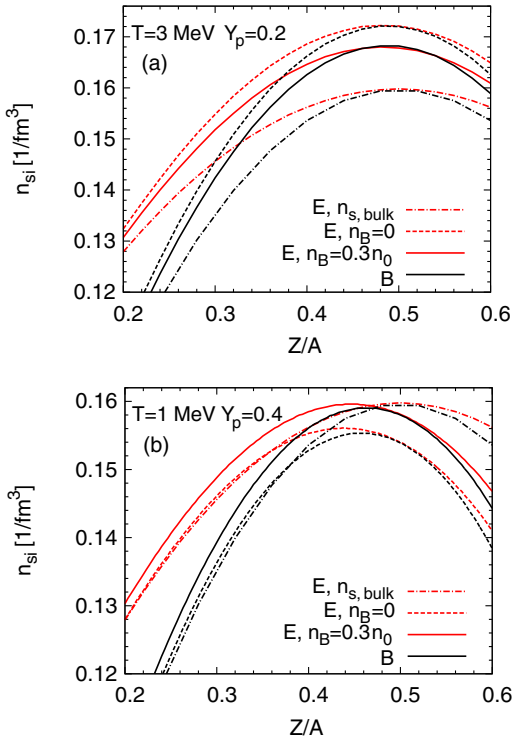

FIG. 10. Equilibrium densities of the nuclei with $A = 50$ (thin) at $(T, Y_p) = (3$ MeV,0.2) (top panel) and 300 (thick) at $(T, Y_p) = (1$ MeV,0.4) (bottom panel) as a function of proton fraction in nuclei, Z/A, for MC models with bulk parameter sets B (black lines) and E (red lines). Solid, dashed, and dashed-dotted lines are those obtained at $n_B = 0.3 n_0$, those at finite temperature and zero density, and those at the density corresponding to the minimum of bulk free energy, $n_{s,\mathrm{bulk}}(Z/A)$, respectively.

are considerably smaller than those in the reference model of the parameter set E, as we expected. This is because the neutron-rich bulk matter has smaller saturation density as described by Eq. (8), thereby resulting in the smaller equilibrium density of neutron-rich nuclei. On the other hand, the qualitative features in the equilibration of individual nuclei are not sensitive to the L parameter; the nuclei are compressed and decompressed for $Y_p = 0.2$ and 0.4, respectively.

IV. CONCLUSION

We have constructed the multinucleus EOS based on the compressible liquid drop model for the stellar matter at subnuclear densities and finite temperatures. The equilibrium densities of individual nuclei are calculated self-consistently. We have compared the single- and multinucleus descriptions, in which the free energies are minimized for nuclear structure and for the nuclear ensemble, respectively. We have found that in-medium nuclei are compressed because Coulomb energies are reduced by background electrons under the condition that few vapor nucleons are present ($X_n + X_p \lesssim 0.05$–0.15), e.g., at $Y_p = 0.4$. But dripped nucleons reduce the surface free energies and induce decompressions of nuclei at a neutron-rich condition such as $Y_p = 0.2$. The average equilibrium density decreases as the baryon density increases regardless of whether

equilibrium densities of individual nuclei are compressed or decompressed, since the nuclei with larger mass numbers and smaller equilibrium densities dominate in the ensemble. We have found that the properties of nuclei are affected to some degree by the compression or decompression even at low baryon densities around $n_B \sim 0.01 n_0$, although the noticeable changes in binding energies, total mass fractions, and average mass numbers are found only at densities above $0.1 n_0$. In core-collapse supernova and neutron star mergers, the nuclei are likely to be decompressed due to dripped neutrons, except just before the core bounce of massive stars. We come to the conclusion that the equilibrium densities of nuclei used in some single-nucleus EOS calculations—see, e.g., [16,29,30]—may be significantly underestimated due to the incorrect density of vapor nucleons. This means that the SNA may not be realistic enough to derive reliable information about in-medium effects as a function of n_B, T, Y_p.

Our model is not perfect because it neglects nuclear forces and Pauli blocking among free nucleons, nuclear shell effects, and light clusters other than the α particle. The Pauli shifts for neutrons would suppress the abundance of nucleons and the impact of surface energy reduction by the neutron vapor may become weak, although the impacts are not so large due to the small neutron fraction for the cases of $Y_p = 0.4$ and/or $T = 3$ MeV. The shell effect should be included and may be affected in medium as well as bulk properties, especially at low temperatures, whereas they are completely washed out at $T \sim 3$ MeV and are negligible. The existence of deuterons and tritons is known to reduce the neutron fraction a little [56], thereby suppressing the surface modification by neutrons. In addition, we should also consider the nuclear pasta phases which are formed above $n_B \gtrsim 0.3 n_0$ yet neglected in this study. As a next step, we plan to address deformations of nuclei including those nuclear pasta phases in MNA. Note that there remain uncertainties in the estimation of surface energy, such as the formulation of its dependence on the nucleon vapor density and choice of σ_0. They also may affect the results quantitatively to some degree. Nevertheless, we hope that our study will provide helpful information for further improvement of the nuclear EOS required for SN simulations. These in-medium effects may lead to significant changes of the dynamics and weak reaction rates in the core-collapse supernovae and neutron star mergers.

ACKNOWLEDGMENTS

S.F. is thankful to S. Yamada, K. Sumiyoshi, and H. Suzuki for the discussion about the FYSS EOS which made the basis of this study. I.M. thanks S. Typel and M. Hempel for useful discussions regarding in-medium modifications of nuclei. S.F. is supported by Japan Society for the Promotion of Science Postdoctoral Fellowships for Research Abroad No. 28-472. A part of the numerical calculations were carried out on the PC cluster at the Center for Computational Astrophysics, National Astronomical Observatory of Japan.

[1] H.-T. Janka, Annu. Rev. Nucl. Part. Sci. **62**, 407 (2012).
[2] K. Kotake, T. Takiwaki, Y. Suwa, W. Iwakami Nakano, S. Kawagoe, Y. Masada, and S.-i. Fujimoto, Adv. Astron. **2012**, 428757 (2012).
[3] A. Burrows, Rev. Mod. Phys. **85**, 245 (2013).
[4] T. Foglizzo, R. Kazeroni, J. Guilet, F. Masset, M. González, B. K. Krueger, J. Novak, M. Oertel, J. Margueron, J. Faure *et al.*, Pub. Astron. Soc. Australia **32**, e009 (2015).
[5] M. Shibata and K. Taniguchi, Living Rev. Relativity **14**, 6 (2011).
[6] J. A. Faber and F. A. Rasio, Living Rev. Relativity **15**, 8 (2012).
[7] A. R. Raduta, F. Gulminelli, and M. Oertel, Phys. Rev. C **93**, 025803 (2016).
[8] S. Furusawa, H. Nagakura, K. Sumiyoshi, C. Kato, and S. Yamada, Phys. Rev. C **95**, 025809 (2017).
[9] W. R. Hix, O. E. B. Messer, A. Mezzacappa, M. Liebendörfer, J. Sampaio, K. Langanke, D. J. Dean, and G. Martínez-Pinedo, Phys. Rev. Lett. **91**, 201102 (2003).
[10] E. J. Lentz, A. Mezzacappa, O. E. B. Messer, W. R. Hix, and S. W. Bruenn, Astrophys. J. **760**, 94 (2012).
[11] S. Wanajo, Y. Sekiguchi, N. Nishimura, K. Kiuchi, K. Kyutoku, and M. Shibata, Astrophys. J. Lett. **789**, L39 (2014).
[12] Y. Sekiguchi, K. Kiuchi, K. Kyutoku, and M. Shibata, Phys. Rev. D **91**, 064059 (2015).
[13] J. M. Lattimer and F. D. Swesty, Nucl. Phys. A **535**, 331 (1991).
[14] H. Shen, H. Toki, K. Oyamatsu, and K. Sumiyoshi, Nucl. Phys. A **637**, 435 (1998).
[15] H. Shen, H. Toki, K. Oyamatsu, and K. Sumiyoshi, Prog. Theor. Phys. **100**, 1013 (1998).
[16] H. Shen, H. Toki, K. Oyamatsu, and K. Sumiyoshi, Astrophys. J. Suppl. **197**, 20 (2011).
[17] A. Burrows and J. M. Lattimer, Astrophys. J. **285**, 294 (1984).
[18] M. Hempel and J. Schaffner-Bielich, Nucl. Phys. A **837**, 210 (2010).
[19] S. Furusawa, S. Yamada, K. Sumiyoshi, and H. Suzuki, Astrophys. J. **738**, 178 (2011).
[20] A. S. Botvina and I. N. Mishustin, Phys. Lett. B **584**, 233 (2004).
[21] A. S. Botvina and I. N. Mishustin, Nucl. Phys. A **843**, 98 (2010).
[22] N. Buyukcizmeci, A. S. Botvina, and I. N. Mishustin, Astrophys. J. **789**, 33 (2014).
[23] J. P. Bondorf, A. S. Botvina, A. S. Iljinov, I. N. Mishustin, and K. Sneppen, Phys. Rep. **257**, 133 (1995).
[24] S. Furusawa, K. Sumiyoshi, S. Yamada, and H. Suzuki, Astrophys. J. **772**, 95 (2013).
[25] S. Furusawa, K. Sumiyoshi, S. Yamada, and H. Suzuki, Nucl. Phys. A **957**, 188 (2017).
[26] N. Buyukcizmeci, A. S. Botvina, I. N. Mishustin, R. Ogul, M. Hempel, J. Schaffner-Bielich, F.-K. Thielemann, S. Furusawa, K. Sumiyoshi, S. Yamada *et al.*, Nucl. Phys. A **907**, 13 (2013).
[27] G. Shen, C. J. Horowitz, and S. Teige, Phys. Rev. C **83**, 035802 (2011).
[28] S. Typel (private communication).
[29] P. Papakonstantinou, J. Margueron, F. Gulminelli, and A. R. Raduta, Phys. Rev. C **88**, 045805 (2013).
[30] F. Aymard, F. Gulminelli, and J. Margueron, Phys. Rev. C **89**, 065807 (2014).
[31] F. Gulminelli and A. R. Raduta, Phys. Rev. C **92**, 055803 (2015).

[32] S. Furusawa, H. Nagakura, K. Sumiyoshi, and S. Yamada, Astrophys. J. **774**, 78 (2013).
[33] T. Fischer, G. Martínez-Pinedo, M. Hempel, L. Huther, G. Röpke, S. Typel, and A. Lohs, EPJ Web. Conf. **109**, 06002 (2016).
[34] M. Hempel, J. Schaffner-Bielich, S. Typel, and G. Röpke, Phys. Rev. C **84**, 055804 (2011),
[35] M. Oertel, M. Hempel, T. Klähn, and S. Typel, arXiv:1610.03361.
[36] K. Oyamatsu and K. Iida, Prog. Theor. Phys. **109**, 631 (2003).
[37] K. Oyamatsu and K. Iida, Phys. Rev. C **75**, 015801 (2007).
[38] M. B. Tsang, J. R. Stone, F. Camera, P. Danielewicz, S. Gandolfi, K. Hebeler, C. J. Horowitz, J. Lee, W. G. Lynch, Z. Kohley *et al.*, Phys. Rev. C **86**, 015803 (2012).
[39] W. G. Newton, M. Gearheart, D.-H. Wen, and B.-A. Li, J. Phys. Conf. Ser. **420**, 012145 (2013).
[40] J. M. Lattimer and A. W. Steiner, Eur. Phys. J. A **50**, 40 (2014).
[41] K. Hebeler and A. Schwenk, Eur. Phys. J. A **50**, 11 (2014).
[42] P. Danielewicz and J. Lee, Nucl. Phys. A **922**, 1 (2014).
[43] H. Sotani, K. Iida, and K. Oyamatsu, Phys. Rev. C **91**, 015805 (2015).
[44] S. Shlomo, V. M. Kolomietz, and G. Colò, Eur. Phys. J. A **30**, 23 (2006).
[45] J. M. Lattimer and Y. Lim, Astrophys. J. **771**, 51 (2013).
[46] G. Watanabe, T. Maruyama, K. Sato, K. Yasuoka, and T. Ebisuzaki, Phys. Rev. Lett. **94**, 031101 (2005).
[47] W. G. Newton and J. R. Stone, Phys. Rev. C **79**, 055801 (2009).
[48] M. Okamoto, T. Maruyama, K. Yabana, and T. Tatsumi, Phys. Lett. B **713**, 284 (2012).
[49] A. S. Schneider, C. J. Horowitz, J. Hughto, and D. K. Berry, Phys. Rev. C **88**, 065807 (2013).
[50] C. J. Horowitz, D. K. Berry, M. E. Caplan, T. Fischer, Z. Lin, W. G. Newton, E. O'Connor, and L. F. Roberts, arXiv:1611.10226.
[51] T. Maruyama, T. Tatsumi, D. N. Voskresensky, T. Tanigawa, and S. Chiba, Phys. Rev. C **72**, 015802 (2005).
[52] C. Ebel, I. Mishustin, and W. Greiner, J. Phys. G: Nucl. Part. Phys. **42**, 105201 (2015).
[53] B. K. Agrawal, D. Bandyopadhyay, J. N. De, and S. K. Samaddar, Phys. Rev. C **89**, 044320 (2014).
[54] C. Sullivan, E. O'Connor, R. G. T. Zegers, T. Grubb, and S. M. Austin, Astrophys. J. **816**, 44 (2016).
[55] Y. Sekiguchi, K. Kiuchi, K. Kyutoku, M. Shibata, and K. Taniguchi, Phys. Rev. D **93**, 124046 (2016).
[56] K. Sumiyoshi and G. Röpke, Phys. Rev. C **77**, 055804 (2008).